1 **Microbial-Induced Heterogeneity in the Acoustic Properties of Porous Media**
2
3 Caroline A. Davis[1], Laura J. Pyrak-Nolte[2], Estella A. Atekwana[3*],
4 D. Dale Werkema Jr.[4] and Marisa E. Haugen[2]
5
6 1. *Missouri University of Science and Technology, Rolla, MO 65409*
7 2. *Purdue University, West Lafayette, IN 47907*
8 3. *Oklahoma State University, Stillwater, OK 74078*
9 4. *U.S. Environmental Protection Agency, Las Vegas, NV 89119*
10
11 Corresponding author: Tel.: +1 405 744 6358; Fax: +1 405 744 7841
12 Email address: estella.atekwana@okstate.edu
13

14 **Abstract**

15   Acoustic wave data were acquired over a two-dimensional region of a microbial-stimulated
16 sand column and an unstimulated sand column to assess the spatiotemporal changes in a porous
17 medium caused by microbial growth and biofilm formation. The acoustic signals from the
18 unstimulated sample were relatively uniform over the 2D scan region. The data from the
19 biologically stimulated sample exhibited a high degree of spatial heterogeneity in the acoustic
20 amplitude measurements, with some regions of the sample exhibiting a significant increase in
21 attenuation while other regions exhibited a decrease. Environmental scanning electron
22 microscopy showed apparent differences in the structure/texture of biofilm between regions of
23 increased and decreased acoustic wave amplitude. We conclude from these observations that
24 variations in microbial growth and biofilm structure causes heterogeneity in the elastic properties
25 of porous media. Our results suggest that acoustic measurements may provide a semi-
26 quantitative approach for the validation of bioclogging models and numerical simulations.
27 INDEX TERMS: 5102 Acoustic properties, 0416 Biogeophysics, 0463 Microbe/mineral
28 interactions.
29

30 **1.0 Introduction**

31   Bioclogging caused by biofilm development is a phenomenon that can cause significant

32 changes in the physical properties of porous media including porosity and permeability changes

33 that influence fluid flow and transport properties [e.g., *Baveye et al.*, 1998] and remediation

34 efforts. Numerical models and simulations have been developed to qualitatively forecast the

35 change in hydraulic properties of a porous medium from bioclogging [e.g., *Brovelli et al.*, 2009].

36 Bioclogging processes are dynamic and are influenced by many phenomena including initial

37 heterogeneities in biomass distribution as well as the physical properties of the porous medium

38 [e.g., *Brovelli et al.*, 2009]. A major difficulty inherent with experimental modeling approaches

39   is that *in situ* quantitative information from direct observation of biological growth and clogging

40   from field data is difficult to obtain at the appropriate spatiotemporal scales needed for model

41   validation [*Dupin and McCarty*, 2000]. Minimally invasive diagnostic techniques are needed to

42   provide near real-time information of the spatiotemporal distribution of biofilms in porous media

43   for validating predictive models and for monitoring microbial growth *in situ*. Although several

44   studies have investigated the rheological properties of biofilms in laboratory settings [e.g.,

45   *Stoodley et al.,* 1999], it is not known how biofilms affect seismic wave propagation in porous

46   media. Such an understanding is critical for assessing the utility of seismic techniques for

47   imaging biofilm spatial heterogeneity and their effects on porous media in field settings.

48   To date, most biogeophysical investigations have focused on geoelectrical techniques

49   [*Atekwana et al.*, 2006]. Apart from a few studies [e.g., *Williams et al.*, 2005; *DeJong et al.*,

50   2006], less attention has been given to the effects of microbial interactions with geologic media

51   on elastic properties, hence questions remain about the effect of microbial growth and biofilm

52   formation in porous media on acoustic wave propagation in the absence of biomineralization.

53   The work described in this letter investigates the influence of biofilm formation on the

54   spatiotemporal seismic properties of porous media. We show for the first time that variations in

55   biofilm structure/texture cause heterogeneity in acoustic wave attenuation of porous media.

56   **2.0 Materials and Methods**

57   Prismatic experimental columns, measuring 102 mm by 51 mm by 254 mm (width x depth x

58   height), were fabricated using 3.2 mm thick clear acrylic. The columns were wet-packed with

59   coarse grain (0.6-1.18 mm) ASTM 20/30 silica sand (Ottawa, IL). Prior to packing, the sands

60   were washed with deionized (DI) water and disinfected by autoclaving. Columns and accessory

61   equipment were also disinfected by rinsing with a 70% ethanol solution. Prior to saturation with

62   the experimental fluids, the sand-packed columns were saturated with sterile 25% Bushnell Haas

63   (BH) nutrient broth (Becton Dickinson) and baseline acoustic measurements were recorded.

64   After initial background measurements, microbial growth was stimulated in one sand column

65   (biostimulated column) by saturating with 25% BH nutrient broth, 30 mM glucose,

66   *Pseudomonas aeruginosa* PAO1 wild type bacteria culture, and 30 µg/mL Gentamicin antibiotic.

67   The bacteria strain (specifically PAO1 Tn7-Gm-gfp) was obtained from the University of

68   Denmark (Lyngby, Denmark), where previous studies with this bacteria strain have been

69   conducted [e.g., *Pamp and Tolker-Nielsen*, 2007]. The other column (unstimulated column) was

70   used for background measurements and was saturated with 25% BH and Gentamicin antibiotic.

71   The Gentamicin antibiotic was added to both the biostimulated and unstimulated columns to

72   inhibit the growth of microorganisms other than the *P. aeruginosa* in the biostimulated column.

73   **2.1 Acoustic Wave Measurements**

74   A full-waveform acoustic wave imaging system was used to obtain two-dimensional point-by-

75   point maps of the acoustic response of the samples [e.g., *Acosta-Colon et al.*; 2009]. The acoustic

76   imaging system used two water-coupled plane-wave transducers (1 MHz central frequency) for

77   the source and receiver. The columns were placed in a water tank to a depth 2/3 the length of a

78   column, and remained *in situ* at laboratory temperature (22-24 ^{o}C) for the duration of the

79   experiment. Using the acoustic mapping mode (C-scan), computer-controlled linear actuators

80   (Newport 850-B4 and Motion Master 2000) were used to move the source and receiver in unison

81   over a 60 mm by 70 mm region in 5 mm increments. A pulse generator (Panametrics PR1500)

82   was used to excite the source and to receive the transmitted signal from the receiver. At each

83   point in the 2D scan region, a 100 microsecond window of the transmitted signal was recorded

84   and digitized with an oscilloscope (Lecroy 9314L). The entire 2D region was scanned 2-3 times

85   per week for the 29 day duration of the experiment.

86   **2.2 Sampling and Analyses**

87   Fluid samples were collected 1-2 times per week from the bottom valve of the columns. The

88   pH was measured using a bench-top probe immediately after fluids were withdrawn. Upon

89   termination of the experiment, the columns were destructively sampled by withdrawing cores of

90   the wet sand (core diameter ~ 6 mm) in a grid-like fashion (15 mm by 15 mm grid) from the

91   acoustic scan region. The sand cores were used for environmental scanning electron microscopy

92   (FEI Quanta 600 ESEM) to image and characterize the surfaces of the sand grains.

93   **3.0 Results**

94   **3.1 Acoustic Wave Monitoring**

95   A time-frequency analysis [*Nolte et al.*, 2000] was performed to determine the amplitude of the

96   compressional signal at a frequency of 0.5 MHz, i.e., the most probable or dominant frequency

97   of the signals. The 2D acoustic scan images of the transmitted compressional wave amplitude

98   obtained from the biostimulated and unstimulated columns are shown in Figure 1, and the

99   temporal percent change in acoustic wave amplitude relative to Day 1 is shown in Figure 2. The

100   2D scans obtained from the biostimulated column on Day 1 reveal relatively uniform

101   compressional wave amplitude over the scan region. However, by Day 5 significant changes

102   were observed in the biostimulated column and the average amplitudes varied spatially over the

103   scan region. For the biostimulated column, the 2D image obtained on Day 29 exhibited an

104   increase in amplitude in some regions (i.e., Figure 1a; Location A), while other regions showed a

105   decrease in amplitude (i.e., Figure 1a; Location B). This is clearly observed in Figure 2a. Unlike

106   the unstimulated column (Figure 2b), the change in amplitude as a function of time varied with

107   location for the biostimulated column (Figure 2a). Compared to Day 1, locations A-C in the

108   biostimulated column (Figure 2a) initially show a decrease in amplitude of ~40% to Day 5.

109   Thereafter, the amplitudes at locations A and B in the biostimulated column increased reaching

110   initial baseline amplitudes by Day 10. The amplitude at location C also increased after Day 5 but

111   did not return to baseline values. Locations D and E (Figure 2a) show a decrease in amplitudes of

112   ~ 80% by Day 14 and remain relatively steady to the end of the experiment. The relatively small

113   overall variation in amplitude (<20%) relative to Day 1 observed from the unstimulated column

114   is consistent for all of the select data points plotted (Figure 2b; Locations A-E).

115   **3.2 Geochemical Monitoring**

116   The pH values from the biostimulated column steadily decreased from a baseline pH of 7 to

117   near 4.4 on Day 12, and remained at a pH of 4.4 through Day 20 (data not shown). From the

118   unstimulated column, a pH of 7 was consistent throughout the duration of the experiment.

119   **3.3 Sand Surface Imaging**

120   Representative ESEM images from the columns sampled at the end of the experiment are

121   shown on Figure 1c. Samples from an area of increased acoustic amplitude (location A, Figure

122   1a) in the biostimulated column shows a rough textured surface which appears to have a patchy

123   covering of 'biomaterial' over some portions of the sand grain, while on other portions of the

124   image the silica sand surface is clearly visible (panel A, Figure 1c). Rod-shaped bacterial cells

125   are present in this biomaterial, but not clearly distinguishable in this image. The ESEM images

126   of sand sampled from an area of decreased acoustic amplitude (location B, Figure 1a) in the

127   biostimulated column show the surface of a sand grain which appears to be completely covered

128   in a smooth biomaterial, with several holes and void-spaces (panel B, Figure 1c). This image

129   also shows the presence of attached rod-shaped bacteria embedded in this biomaterial. In

130   contrast, the ESEM images of samples obtained from the unstimulated column (location C,

131 Figure1B) show the irregular or hummocky surface of a silica sand grain with no apparent

132 attached bacteria cells or biomass (panel C, Figure 1c).

4.0 Discussion and Conclusions

134 In this study the compressional wave amplitude was observed to differ both temporally and

135 spatially, between the biostimulated and unstimulated columns (Figure 1). Compressional wave

136 amplitudes in the biostimulated column became more spatially variable while the acoustic

137 response of the unstimulated column homogenized over time. While the changes observed in the

138 unstimulated column (<20%) are not insignificant (Figure 2b), they are far less than the

139 measured changes from the biostimulated column and consistent for all of the select data points.

140 Hence we attribute the changes in the latter to particle settling. Except for a few locations (e.g.,

141 Location A, Figures 1a & 2a) that showed an increase, most locations in the biostimulated

142 column showed a decrease in the compressional wave amplitudes over time with some regions

143 decreasing to ~ 80% of Day 1 values (e.g., Location E, Figure 2a). Microbial growth was active

144 in the biostimulated column as evidenced by the decrease in pH (from 7 to 4.4) and ESEM

145 images that confirm microbial cell colonization of sand surfaces (Figure 1c, panels A and B). No

146 microbial growth was observed in the unstimulated column (panel C, Figure 1c). The decrease in

147 pH most likely resulted from the accumulation of metabolic byproducts such as organic acids

148 [e.g., *Silverman and Munoz*, 1974], which eventually inhibited continued microbial growth in the

149 columns.

150 The bacteria culture used in this study (*P. aeruginosa*) is capable of producing different types

151 of biofilms, depending on the environment [e.g., *Friedman and Kolter*, 2004], and formation of

152 these biofilms is documented to occur in different stages [e.g., *Davey et al.,* 2003]. Initial stages

153 in the formation of *P. aeruginosa* biofilms are characterized by the attachment of planktonic

154   cells to solid surfaces. Initial attachment is followed by colonization of the surfaces followed by

155   the production of extrapolymer substances (alginate - a viscous gum) that embed the reproducing

156   cells allowing them to form microcolonies and build thick biofilms. One characteristic of the *P.*

157   *aeruginosa* biofilms described in the literature [e.g., *Davey et al.*, 2003; *Pamp and Tolker-*

158   *Nielsen*, 2007] is the presence of macrocolonies surrounded by large void spaces or open, dark

159   fluid-filled channels, through which the lower levels of bacteria in the biofilm are thought to

160   dispose of accumulating waste products (e.g., see panel B, Figure 1c). The ESEM images (panel

161   A and B, Figure 1c) obtained from the biostimulated column show apparent qualitative

162   differences in the texture of the attached biofilm between areas of increased and decreased

163   amplitude. We hypothesize that differences in the measured amplitudes reflect differences in the

164   structure/texture of the attached biofilms in the biostimulated column.

165   Acoustic properties of porous media are generally dependant on the bulk modulus of the

166   saturating fluid [e.g., *Knight and Nolen-Hoeksema*, 1990], the elastic moduli of the solid media

167   [e.g., *Ecker et al.*, 1998], and the solid-fluid interactions [e.g., *Clark et al.*, 1980]. Energy loss

168   mechanisms for fluid-saturated porous media fall into three categories: viscoelastic loss, fluid-

169   solid surface physiochemical loss, and scattering loss [*Li et al.*, 2001]. Generally, decreases in

170   acoustic amplitude result from biogenic gas production or the weakening of grain contacts

171   (physical/chemical alteration of surfaces and/or grain contacts [e.g., *Murphy et al.*, 1984; *Clark*

172   *et al.*, 1980]) in porous media, both of which reduce the elastic moduli and are manifested by

173   delays and attenuation of acoustic waves. We observed no gas bubble formation in the

174   biostimulated column. Hence, we hypothesize that the presence of biofilms caused the changes

175   in elastic properties of the sample which is consistent with studies that suggest that soft and

176   patchy structures like biofilm surfaces result in the effective attenuation of sound [e.g., *Janknecht*

177 *and Melo*, 2003].

178   Increases in acoustic amplitude may result from increases in the bulk modulus of the solid

179 media [e.g., *Li et al.*, 2001] through the stiffening of grain contacts. Hence it is possible that in

180 the regions of increased amplitude, the extrapolymer substances resulted in enhanced coupling

181 between grains, whereas areas of decreased amplitude may be explained by viscous losses or

182 physiochemical alterations at grain contacts due to the nature of the biofilms. We note that

183 during ESEM imaging of the sand samples from regions with increased amplitude (Figure 1a;

184 Location A), individual bacterial cells were not clearly distinguishable until the operating

185 temperature of the ESEM was raised from 5 to 20°C, and the relative humidity was decreased

186 from 89% to 14%, which effectively dried out the sample/biomaterial. However, individual cells

187 and attached biomass on sand samples collected from Location B (Figure 1a), were evident

188 immediately upon viewing with the ESEM (at 5°C and 89%) and remained virtually the same in

189 appearance when the temperature was increased to 20°C (images not shown).

190   Wave scattering or interference from spatial heterogeneity of the medium is another

191 mechanism that affects wave attenuation. The biostimulated sample did not exhibit biogenic gas

192 formation, which suggests that air bubbles are not a source of scattering. The density contrast

193 between water-saturated sediment and the biofilm-microbially altered sediment is not large.

194 Thus, a potential source of scattering is a spatial variation in elastic or viscoelastic moduli from

195 microbial alteration of the grain contact, pore-filling material and/or biofilm connecting grains.

196   Our investigation shows that acoustic imaging techniques are sensitive to spatiotemporal

197 changes in porous media caused by enhanced microbial growth of a biofilm forming bacteria

198 culture. While the exact microbial-induced mechanisms for the variations in amplitude are yet

199 unclear, we speculate that the differences in amplitude arise from a non-uniform distribution of

200 microbial activity or possible heterogeneity in the biomass distribution and biofilm morphology.

201 The applicability of our laboratory measurements to the field scale will depend on spatial and

202 temporal dispersion. Temporal dispersion connects frequency-dependent attenuation and velocity

203 with elastic moduli, i.e. changes at grain contacts or pore-filling. Spatial dispersion connects

204 wavelength with the size of the scatterer, i.e., the size and/or spatial correlation length of

205 microbially altered regions. Increasing or decreasing attenuation with frequency will provide

206 information on the size of the altered region and on the spatiotemporal distribution of

207 biomass/bioclogging development.

208 **Acknowledgements**

217 **References**

219 Acosta-Colon, A., L. J. Pyrak-Nolte, and D. D. Nolte (2009), Laboratory-scale study of field of
220   view and the seismic interpretation of fracture specific stiffness, *Geophys. Prospect.*, *57*(2),
221   209-224.
222 Atekwana, E. A., E. A. Atekwana, and D.D. Werkema (2006), Biogeophysics: the effects of
223   microbial processes on geophysical properties of the shallow subsurface, in *Applied*
224   *Hydrogeophysics*, edited by H. Vereecken, A. Binley, G. Cassiani, A. Revil, and K. Titov, pp.
225   161-193, NATO Sci. Ser. IV, Springer, New York.
226 Baveye, P., P. Vandevivere, B. L. Hoyle, P. C. DeLeo, and D. Sanchez de Lozada, (1998),
227   Environmental impact and mechanisms of the biological clogging of saturated soils and aquifer
228   materials, *Crit. Rev. Environ. Sci. Tech., 28*(2), 123-191.

229 Brovelli, A., F. Malaguerra, and D. A. Barry, (2009), Bioclogging in porous media: Model
230   development and sensitivity to initial conditions, *Environmental Modelling and Software*, *24*,
231   611-626.
232 Clark, V. A., B. R. Tittman, and T. W. Spencer, (1980), Effect of volatiles on attenuation (Q-1)
233   and velocity in sedimentary rocks, *J. Geophys. Res., 85*, 5190-5198.
234 Davey, M. E., N. C. Caiazza, and G. A. O'Toole (2003), Rhamnolipid surfactant production
235   affects biofilm architecture in Pseudomonas aeruginosa PAO1, *J. Bacteriol., 185*(3), 1027-
236   1036, doi:10.1128/JB.185.3.1027–1036.2003.
237 DeJong, J. T., M. B. Fritzges, and K. Nusslein (2006), Microbially induced cementation to
238   control sand response to undrained shear, *J. Geotech. Geoenviron. Eng.*, *132*(11), 1381-1392.
239 Dupin, H. J., and P. L. McCarty (2000), Impact of colony morphologies and disinfection on
240   biological clogging in porous media, *Environ. Sci. Technol., 34*(8), 1513-1520;
241   doi:10.1021/es990452f.
242 Ecker, C., J. Dvorkin, and A. Nur (1998), Sediments with gas hydrates: internal structure from
243   seismic AVO, *Geophysics, 63*, 1659-1669.
244 Friedman, L., and R. Kolter (2004), Genes involved in matrix formation in Pseudomonas
245   aeruginosa PA14 biofilms, *Molec. Microbio., 51*(3), 675–690 doi:10.1046/j.1365-
246   2958.2003.03877.x.
247 Janknecht , P and L. F. Melo (2003), Online biofilm monitoring, *Rev. in Env. Sci. and
248   Bio/Techn., 2,* 269–283.
249 Knight, R., and R. Nolen-Hoeksema, (1990), A laboratory study of the dependence of elastic
250   wave velocities on pore scale fluid distribution, *Geophys. Res. Lett., 17*, 1529-1532.
251 Li, X., L. R. Zhong, and L. J. Pyrak-Nolte (2001), Physics of partially saturated porous media:
252   residual saturation and seismic-wave propagation, *Ann. Rev. Earth Planet. Sci., 29*, 419-460.
253 Murphy III, W. F., K. W. Winkler, and R. L. Kleinberg (1984), Frame modulus reduction in
254   sedimentary rocks: the effect of adsorption on grain contacts, *Geophys. Res. Lett.*, *1*(9), 805-
255   808.
256 Nolte, D. D., L. J. Pyrak-Nolte, J. Beachy, and C. Ziegler (2000), Transition from the
257   displacement discontinuity limit to the resonant scattering regime for fracture interface waves,
258   *International Journal of Rock Mechanics and Mining Sciences*, *37*(1-2), 219-230.
259 Pamp, S. J., and T. Tolker-Nielsen (2007), Multiple roles of biosurfactants in structural biofilm
260   development by Pseudomonas aeruginosa, *J. Bacteriol., 189*(6), 2531–2539,
261   doi:10.1128/JB.01515-06.
262 Silverman, M. P., and E. F. Munoz (1974), Microbial metabolism and dynamic changes in the
263   electrical conductivity of soil solutions: A method for detecting extraterrestrial life, *Appl.
264   Microbiol.*, *28*(6), 960– 967.
265 Stoodley, P., Z. Lewandowksi, J. D. Boyle, and H. M. Lappin-Scott (1999), Structural
266   deformation of bacterial biofilms caused by short-term fluctuations in fluid shear: an in situ
267   investigation of biofilm rheology, *Biotech. Bioeng., 65*(1), 83-92.
268 Williams, K. H., D. Ntarlagiannis, L. D. Slater, A. Dohnalkova, S. S. Hubbard, and J. F.
269   Banfield, (2005), Geophysical imaging of stimulated microbial biomineralization, *Environ. Sci.
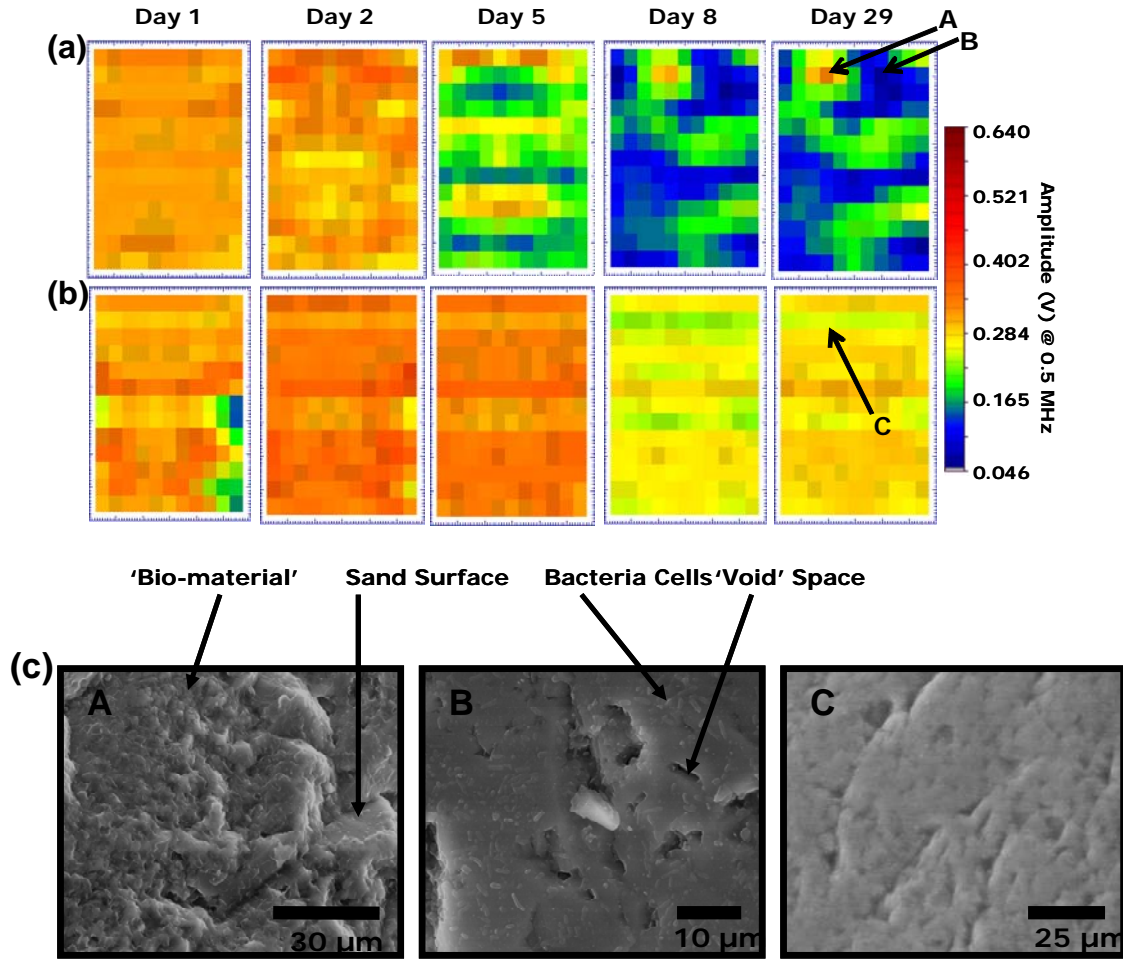270   Technol., 39*(19), 7592-7600.
271

Figure 1: 2D acoustic wave amplitude scans (at 0.5 MHz) from the (a) biostimulated and (b) unstimulated columns for Days 1, 2, 5, 8, and 29. Black letters (A,B,C) on Day 29 of the 2D scans denotes location of ESEM images shown in (c): panel (A) is from the biostimulated column from an area of increased amplitude; panel (B) is from an area of decreased amplitude; and panel (C) is from the unstimulated column with no apparent attached biomass. Note the differences in the texture of the attached biomass between (A) having a rough texture and (B) smooth texture with the grain surfaces completely covered by biomaterial.
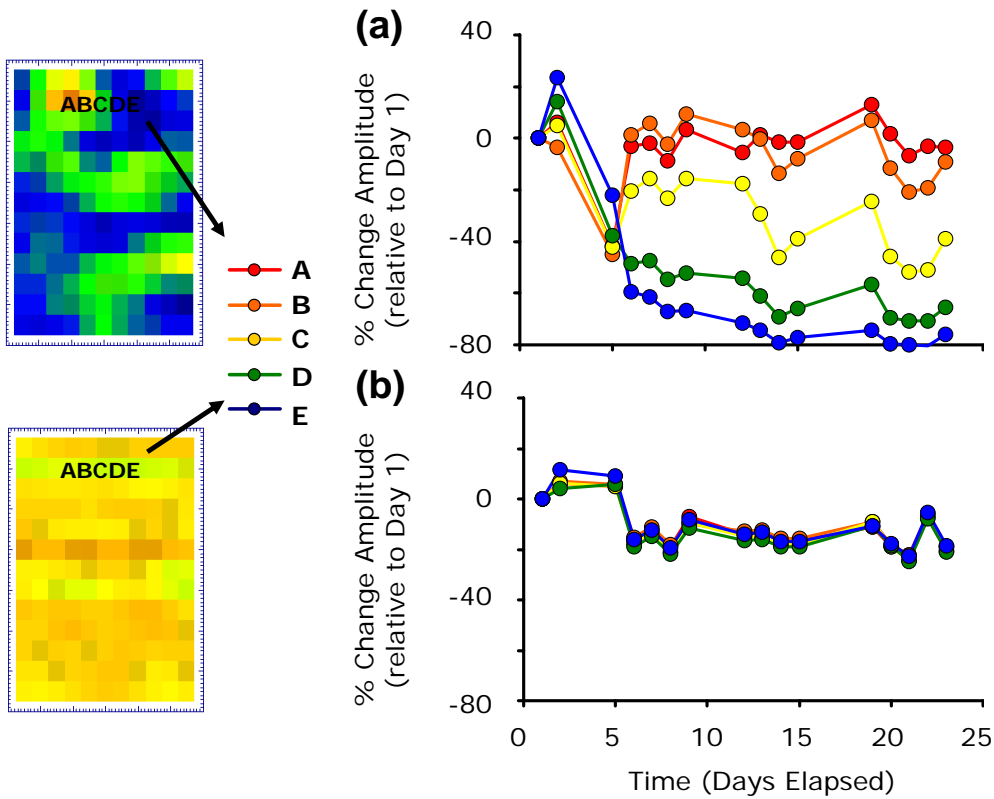
Figure 2: Graphs showing the temporal percent change in acoustic wave amplitude (at 0.5 MHz) relative to Day 1 for the (a) biostimulated and (b) unstimulated columns. Note the significant increase in attenuation (~80 %) for the biostimulated compared to the unstimulated sample (~20 %).